

SAR INTERFEROMETRY FOR LANDSLIDE INVESTIGATION AND SURFACE DEFORMATION MONITORING: A CASE STUDY OF SOUK AHRAS AREA, NORTH-EAST OF ALGERIA

Nour El Houda Gueraidia, Saida Gueraidia, Chemseddine Fehdi

Summary

Landslides – natural disasters be caused by various factors - are frequent in the region surrounding Souk Ahras. Comprehensive fieldwork, such as geotechnical drilling investigations and soil excavations, is conducted to monitor ground movements and assess the feasibility of geological locations. Synthetic Aperture Radar (SAR) and other active satellite remote sensors are utilized in Earth Observation-based systems to identify and track ground deformation and landslides in the study area. This research aims to illustrate how open-source processing software, SNAP, provided by the European Space Agency, can be combined with freely available datasets from Copernicus to accomplish this goal. In the North Eastern part of Algeria, which includes Souk Ahras, there is a high risk of landslides Through the use of InSAR technology, the research provided satisfactory results in identifying the morphology of landslides and generating a large-scale interferometric map covering several regions in the East of Algeria, revealing the extent of distortion and spacing caused by the landslide phenomenon.

Keywords

InSAR • SAR • interferometry • landslides • deformation • Zaarouria • Hammam Tassa • Mevhrouha

1. Introduction

Due to the mountainous terrain and steep slopes, landslides are one of the most common threats in the eastern Algerian state of Souk Ahras. As a result, the best way to identify potential risk of landslides is to monitor surface movement over a large area.

However, depending on the inventory's purposes, scales, data gathering techniques, and attributes of the imagery that is available, landslide maps may have various resolutions and levels of information [Cruden et al. 1996, VanWesten 2006]. For precisely these reasons, advanced techniques and cutting-edge technology assist in overcoming some of the weaknesses of traditional mapping processes. The modern application of numerous remote sensing technologies, including Synthetic Aperture Radar (SAR),

optical measurements, Light Detection and Ranging (LiDAR), represents valuable complementary data sources compared to conventional mapping and monitoring methods. New technologies and developing space industry will consume less time and funds to update landslide inventories over large areas. In the past decade, the use of InSAR techniques for detecting and monitoring long-term mass movements has been well documented for numerous landslide typologies due to its large spatial coverage, high spatio-temporal resolution, and ability to work in all weather conditions.

For instance, the conventional differential InSAR approach has been used to track slow landslides that move at a rate of dm/yr [Guzzetti et al. 2000, Frangioni et al. 2014].

The principal objective of this project is to demonstrate how techniques based on SAR satellites can be used to identify and track ground motion associated with landslides.

The method is especially helpful for slow-moving landslides and vast areas, where using ground-based surveying is impractical [Akbarimehr et al. 2013, Bovenga et al. 2012, Colesanti and Wasowski 2006, Haghshenas Haghghi and Motagh 2016, Tong and Schmidt 2016, Wasowski and Bovenga 2014, Raucoules and de Michele 2020].

The InSAR technique encounters challenges, when there are spatial and temporal decorrelations due to vegetation coverage, uneven terrain, substantial deformations, or phase artifacts caused by the atmosphere [Hanssen 2001, Singleton et al. 2014, Tang et al. 2015, Yun et al. 2007].

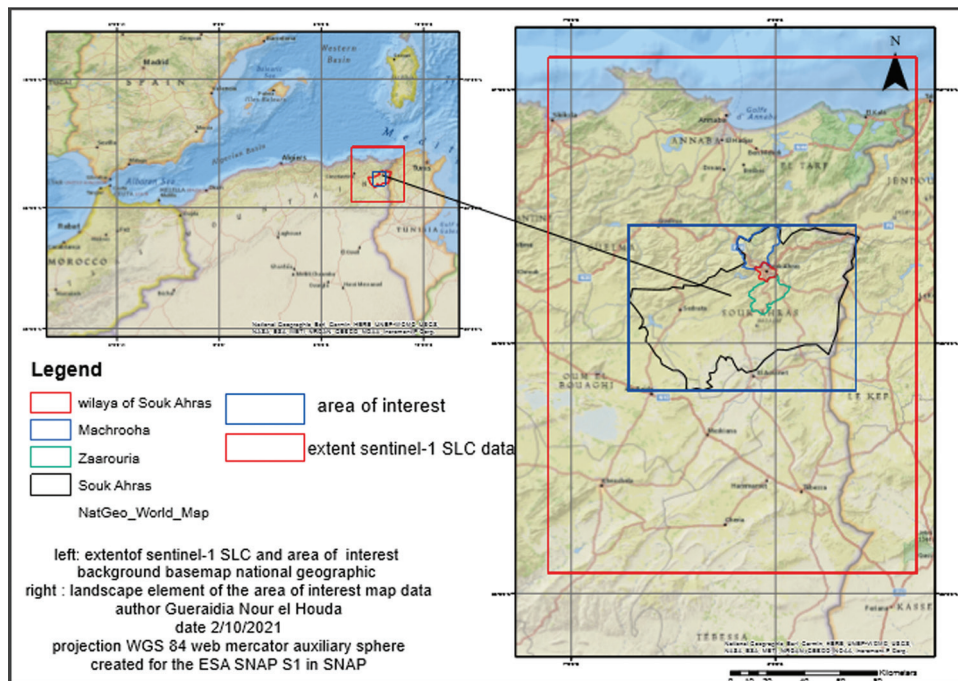
A multiscale approach must be used for spatial optimization of this type of warning system, which helps to minimize the area to be monitored [Niemeier and Riedel 2006]. The processing of remote sensing data is the first phase in this multiscale approach or observation concept, as it is the most important step in the early identification of high-risk areas. Remotely sensed data can be used as a starting point for current and future satellite missions to identify and monitor processes at the Earth's surface, while also allowing scientists to evaluate historical evidence of landslides. We studied the potential of the Synthetic Aperture Radar Interferometry for detecting surface motions at various test sites.

2. Description of the study area

The study area is located in eastern Algeria, one of the most landslide-prone areas in the country. The Souk Ahras area lies between latitude: 36°17.1834' N and longitude: 7°57.0666' E (Fig. 1).

The study area is mountainous with rugged topography, Souk Ahras province in eastern Algeria lies on the Tunisian border in the east, El Tarf and Guelma in the north, Oum El Bouaghi in the southwest, and Tebessa in the south. It is situated in a depression surrounded by wooded mountains on either side; mountains which are attacked by interests and penetrated by Mjarda valley. The province of Souk Ahras has an area of 4360 km². It is divided into 10 districts and 26 municipalities occupied by 453 917 people, representing 0,18% of the entire national territory. Its climate is semi-dry and contains two large dams, Ain Dalia Dam and Oued Chief, with a total capacity of over

240 million m³. Souk Ahras municipality itself is the most vulnerable area to landslides in the whole province.



Source: Authors' own study

Fig. 1. Map of localisation of Souk Ahras area

The region has a Mediterranean climate with two seasons: a dry season that begins in May and lasts until October, and a rainy season that lasts from November to April. Most of the SM occur in the first season. The annual rainfall average varies from ~700 mm in the lowlands of the south, north, and east to ~1200 mm on the western peaks of Jebel Rezgoune [Kabouya 1990]. High-altitude areas are covered in snow throughout the winter.

Due to the study area's morphology, which makes it susceptible to landslides and floods, natural disasters and hazards occur there frequently. Floodings created by rain that result in rivers overflowing, flash floods and landslides are the main causes of disasters in this area, with the study area's morphology being the secondary cause. This area is characterized by a dissymmetry of the relief, which appears transversely with a slope NW. And also by an altitude that decreases regularly towards the SW, and by anticlinal structures NE-SW, in the sector of Taoura.

2.1. Geology

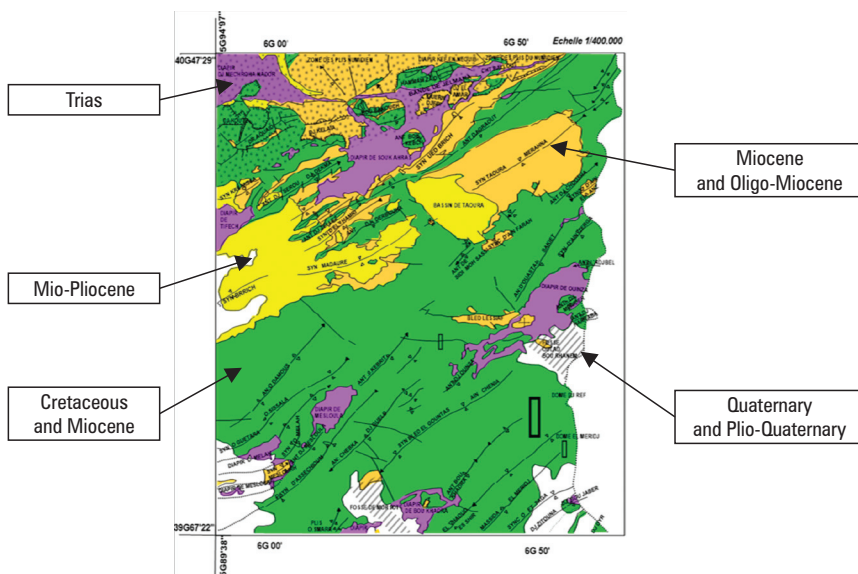
The geology of the discussed area was studied by several authors [Vila 1980]. The geological structures have shown that the studied region presents very heterogeneous geology, characterized by sedimentary formations, the oldest age of which varies from Triassic to Quaternary, and are generally constituted by limestones, sandstones, marls, and pebbles and alluvium. It is a border zone between the Tellian Atlas in the north and the Saharan Atlas in the south.

In the north the area of Souk Ahras is covered by alluvial grounds made up of units of the internal domain, such as flyshs, and of the external domain; in the south and the east by an intensely folded and fractured unit of the atlasic region foreland.

The region is characterized by two primary structural directions: the first, NE-SW with Triassic extrusions, and the second, NW-SE, with WNW-ESE, marked by distensive movement during post-Miocene collapse.

A succession of synclinal and anticlines bored at their edges by a diapiric formation run in the SW-NE direction, and are cut by two fault systems: one consists major sub-parallel faults with the axes of collapsing anticlines. The dips are inversely sub-vertical. This system is directed in two major tectonic directions: The North-East (30-60°) and the North-West (280-320°).

The other system consists of second-order faults runs almost perpendicular to the principal system. It is characterized by important discards and dips, about 60° in the East-West direction (Fig. 2).



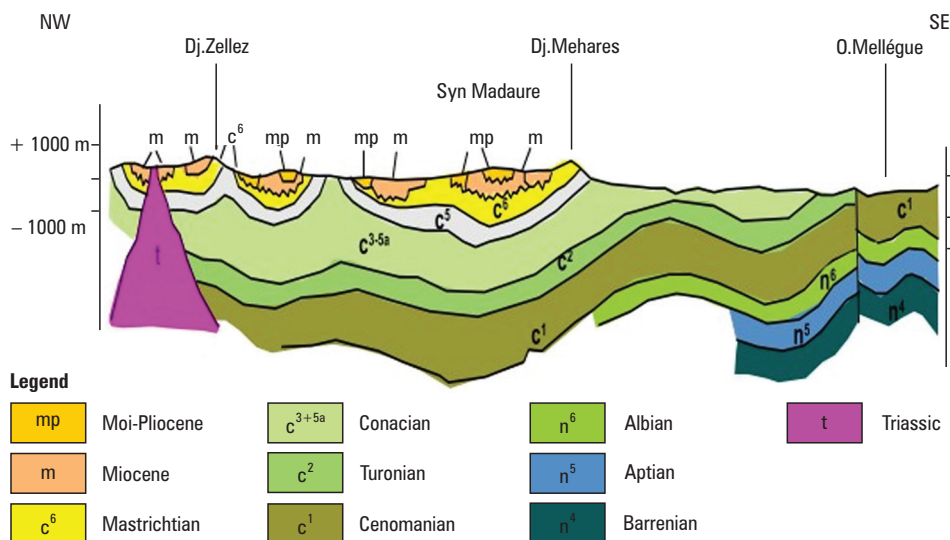
Source: Authors' own study

Fig. 2. The geological formations presented on the geological map of the study area

According to geological maps covering the territory of the Souk-Ahras district, a lithological map at 1/50000 was established to serve as a basis for the pedologic map. It reflects the lithological nature of the large geological formations encountered, which range from the Triassic, being the oldest formation, to the most recent, Quaternary terrains of the stratigraphic scale summarized in Table 1 and Figures 2-3.

Table 1. Representation of the stratigraphic scale

Age	Dominant lithology
Quaternary	Alluvium, terraces
Terraces	Continental Mio-Pliocene-Red clays, sands, agglomerates
Late Miocene	Clays and sandyclays
Early Miocene	Sandy clays, lacustrine clays and limestones
Oligocene	Red clays and sandy clays from Numidia
Middle Eocene	Marls and limestonesheets
Early Eocene	Marls and limestonesheets
Late Cretaceous	Senonianlimestone and marls
Early and Middle Cretaceous	Turonian marl and marl limestone
Triassic	Marls Gypsum, limestone and dolomite

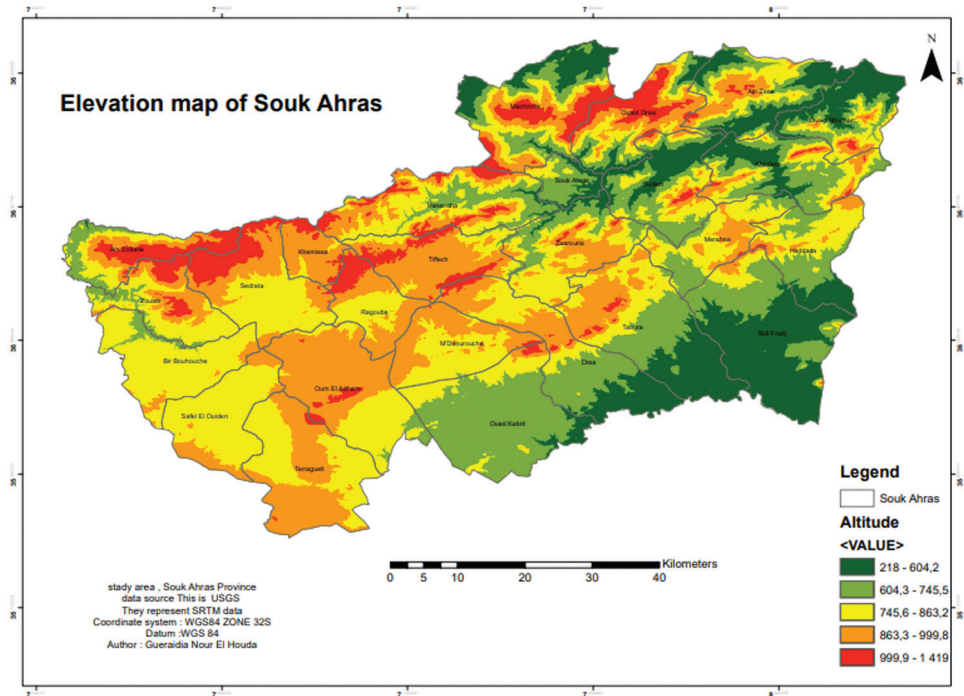


Source: Authors' own study

Fig. 3. Geological section of the Souk Ahras region

2.2. Topography

The study area includes two depressions facing the east. Its altitude varies between 462 m in the bed of the Medjerda wadi and 1098 m in the mountains in the center of the studied region (the highest peak of the study area is the Djebel Chouga at hammam Tassa, 1098 m) (Fig. 4).



Source: Authors' own study

Fig. 4. Elevation map of study area

2.3. Hydrography and water resources

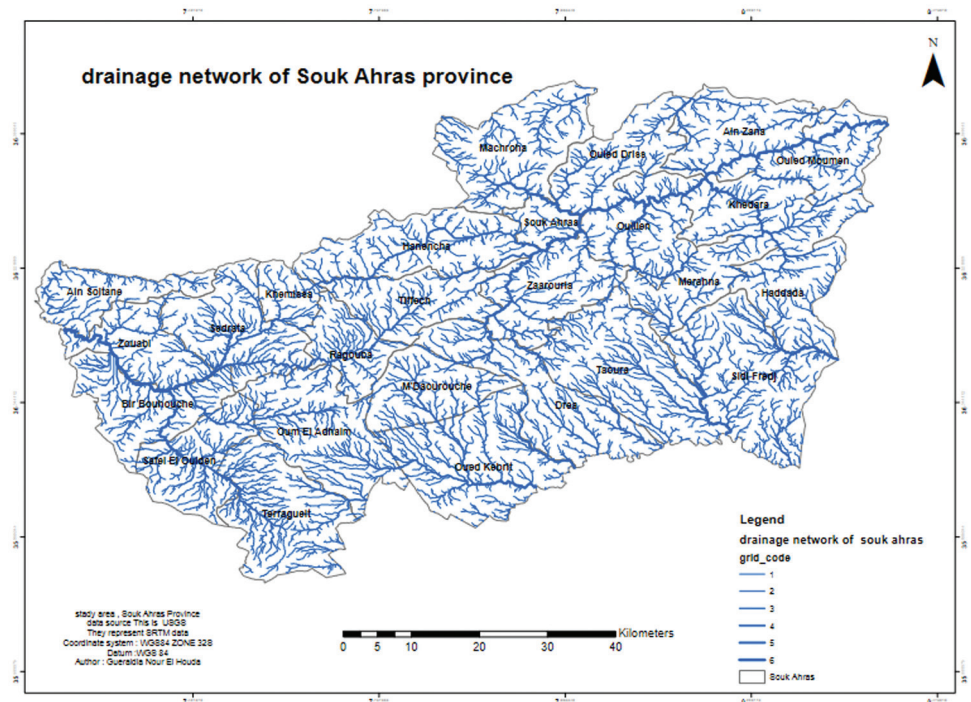
Located in the middle of the watershed Medjerda-Mellegue area, the region of Souk Ahras is rich in water resources. The groundwaters concentrate mainly in the Taoura and Terreguellt groundwater table. The surface waters are particularly collected by the Ain Dalia dam (Fig. 5).

The main watercourses crossing the basin are: Medjerda wadi, Mellegue Wadi, Echaref Wadi, and Wadi Laghdir [Mebarki 2003].

The Maastrichtian-Danian limestones contain a karstic system, which supplies multiple downstream springs [Masrouhi 2008].

The hydrographic network is forced to flow in two preferred ways by the morpho-tectonic topographic model: one towards the east, which is determined by the fold

structure, and the other towards the north, which is determined by the overall topographic slope [Mebarki 2005].



Source: Authors' own study

Fig. 5. Hydrological map of study area

From the upstream to the downstream, it is difficult for many wadis to maintain their connections with the principal artery of the basin. The layout of the wadis is often perpendicular to the folds [Chouabi 1987].

3. Types of Landslides in the study area

The term 'landslide' refers to a wide range of processes that cause the outward and downward movement of slope-forming materials, such as rock, soil and artificial fill, or a mixture of these materials. The components may shift by toppling, slipping, spreading, or flowing. The types of material involved and the movement can be used to distinguish between many types of landslides. Table 2 displays a classification scheme based on these criteria. Other classification systems take into account further factors, such as the rate of movement and the amount of water, air, or ice in the landslide debris. Rotational sliding is the most common form in the Souk Ahras area (Fig. 6).

Table 2. Types of landslides. Abbreviated version of Varnes' classification of slope movements [Varnes 1978]

Type of movement	Type of material		
	Bedrock	Engineering soils	
		Predominantly Course	Predominantly Fine
Falls	Rock fall	Debrisfall	Earthfall
Topples	Rock topple	Debris topple	Earth topple
Slides	Rock slide	Debris slide	Earth slide
	Translational		
Lateral Spreads	Rock spreads	Debris spreads	Earth spreads
Flows	Rock flow (Deep creep)	Debris flow (Soil creep)	Earth flow (Soil creep)
Complex	Combination of two or more principal types of movement		



Source: Authors' own study

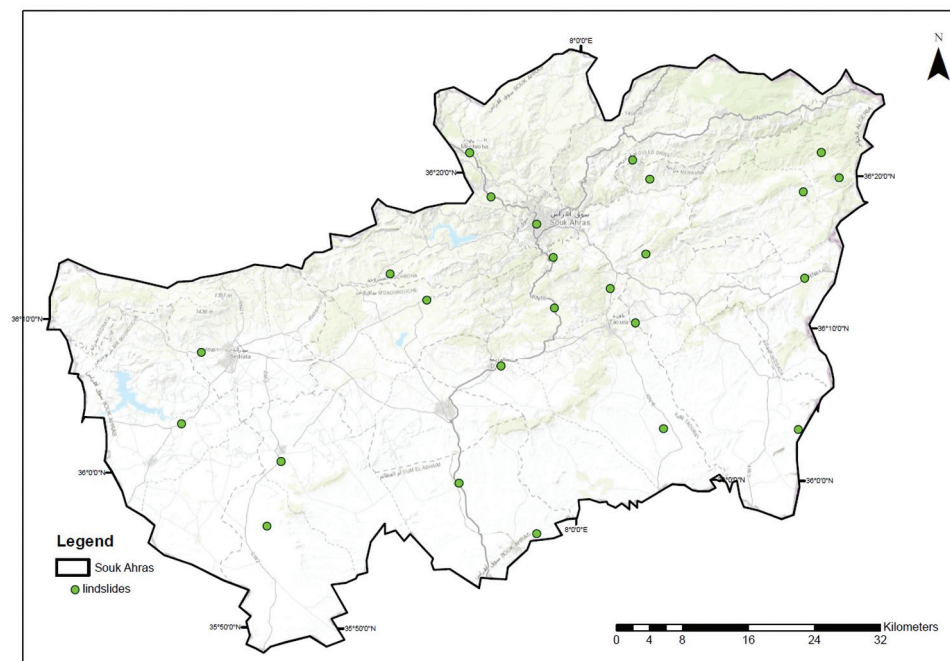
Fig. 6. Location of some landslide in the study area on Google Earth: a) landslides of Hammem Tassa $36^{\circ}14'59.29''N$ $8^{\circ}1'33.57''E$; b) landslides of Zaarouria $36^{\circ}13'44.49''N$ $7^{\circ}57'41.92''E$; c) landslides of Machrouha $36^{\circ}21'15.45''N$, $7^{\circ}50'39.06''E$

Disturbances in the inherent stability of slopes lead to landslides. They may come after droughts, earthquakes, and strong rains. When water rapidly builds up in the ground, a surge of water-soaked rock, earth, and debris occurs, causing mudslides [Hadji et al. 2017].

Because water changes the pressure within the slope, which results in slope instability, it can induce landslides and mudslides. As a result, the heavy slope elements (soil, rock, etc.) that are saturated with water will be overcome by gravity. According to theory, one of the most common causes of landslides is excess of water.

The development of the susceptibility map requires an inventory before landslides in the study area. Our inventory was carried out using the satellite map of the study region with field work (Fig. 7). This inventory is necessary to determine the existence

of these instabilities and also to search for the average factors and the critical values of these movements.



Source: Authors' own study

Fig. 7. Landslide inventory map of the study area

4. Landslide inventory

The identification of landslide processes, including their spatial distribution and properties like geometry, volume, and total area as well as their causes, recurrence rates, and sliding rates during prior landslide activity, are displayed on maps and databases. The combined use of InSAR-derived deformation maps and DEM gradient maps is also an effective and systematic technique for identifying likely active slow-moving landslide candidates by establishing a threshold of topographic slopes based on in-situ geological research (Fig. 7).

5. Material and methods

5.1. SAR interferometry

5.1.1. Basic principles

The early use of satellite-based InSAR utilized Sea sat data in the 1980s, but the 1990s saw the launch of ERS-1 (1991), JERS-1 (1992), RADARSAT-1, and ERS-2, which

increased the technique's capability (1995). These platforms provided the InSAR-required short baselines, stable orbits, and well-defined orbits. More recently, during the 11-day NASA STS-99 mission in February 2000, a SAR antenna mounted on the space shuttle was used to gather data for the Shuttle Radar Topography Mission. ESA launched the ASAR sensor aboard Envisat in 2002 to replace the ERS.

While most InSAR missions to date have used C-band sensors, more recent missions like ALOS PALSAR, TerraSAR-X, and COSMO SKY MED are increasing the amount of data that is currently available in the L- and X-band (Figs. 8, 9).



Source: Authors' own study

Fig. 8. Sentinel-1 radar vision



Fig. 9. Some parameters of the radar beam: a) TerraSAR-X; b) COSMO-SkyMed Seconde Génération (CSG); c) image of the Advanced Land Observing Satellite 'DAICHI' (ALOS)

5.2. Datasets

SAR images were taken before and after the D-InSAR technology was applied in order to examine deformations induced by landslides in the greater area of Souk Ahras district.

As a result, two Sentinel-1 SAR photos were obtained, one on 10 June 2020, and the other on 23 February 2021. The features of the obtained photos are presented in Table 3.

Table 3. Sentinel-1 synthetic aperture radar (SAR) image characteristics.

Name	S1B_IW_SLC__1SDV_20210223T172814_20210223T172844_025737_03117A_1F4D	S1A_IW_SLC__1SDV_20200610T172841_20200610T172908_032958_03D14B_03FA
Date	23-FEV-2021	10-JUN-2020
Instrument	SAR-C	SAR-C
Mode	Interferometric Wide swath (IW)	Interferometric Wide swath (IW)
Satellite	Sentinel-1	Sentinel-1
Cycle Numbers	45	46
Orbit Numbers	32958	21887
Pass direction	ASCENDING	ASCENDING
Polarization	VV VH	VV VH
Product level	L1	L1
Product type	Single Look Complex (SLC)	Single Look Complex (SLC)
Relative orbit	161	161

The open-source program Sentinel Applications Platform was used to process the pair of images (SNAP). Following data analysis, it is possible to establish that distinct sections of land have experienced significant movement during the observation period.

To provide a more precise estimate for this investigation, Sentinel 1A images will also be used to observe the geodynamic activity of the area's geological environment.

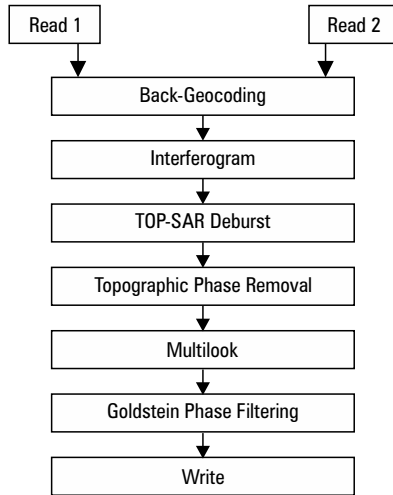
The Sentinel-1 satellite's SAR sensor offers dual-polarization operation (HH-HV, VV-VH), which can be utilized to improve the spatial density of data points using the polarimetric optimization method.

This study evaluates the advancement in displacement mapping by incorporating data from the Sentinel-1 VH channel into the PS-InSAR analysis.

5.3. Steps for InSAR processing

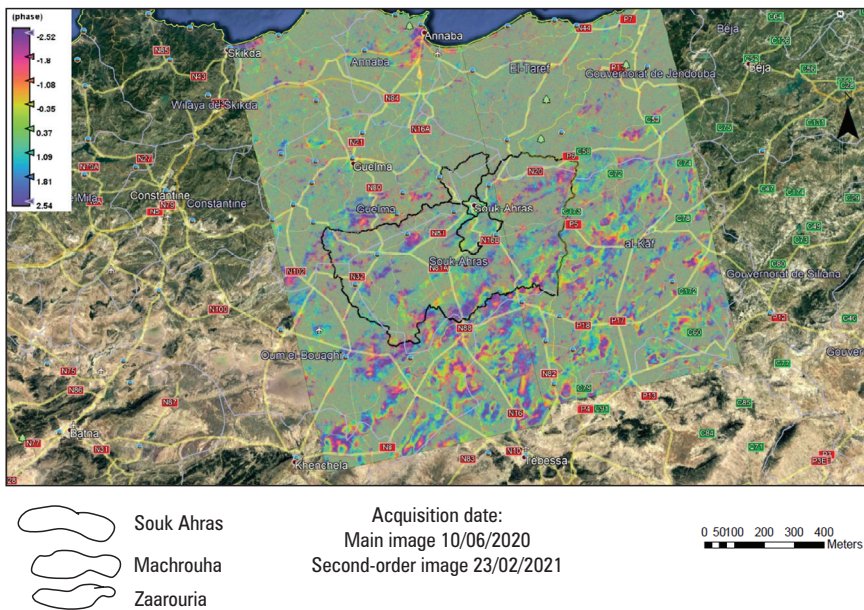
5.3.1. Create an interferogram

By cross-duplicating the ace picture with the slave's complex conjugate, an interferogram is created. While the stage relates to the contrast between the two images, the sufficiency of both photographs is duplicated. In the course of the Interferogram Arrangement step, the flat-earth stage is consequently eliminated. Due to the changing of the reference surface, the stage indicated within the interferometry flag is the flat-earth stage. Using orbital and metadata information, the flat-earth stage is assessed and subtracted from the complicated interferogram (Fig. 10).



Source: Authors' own study

Fig. 10. Interferogram formation steps

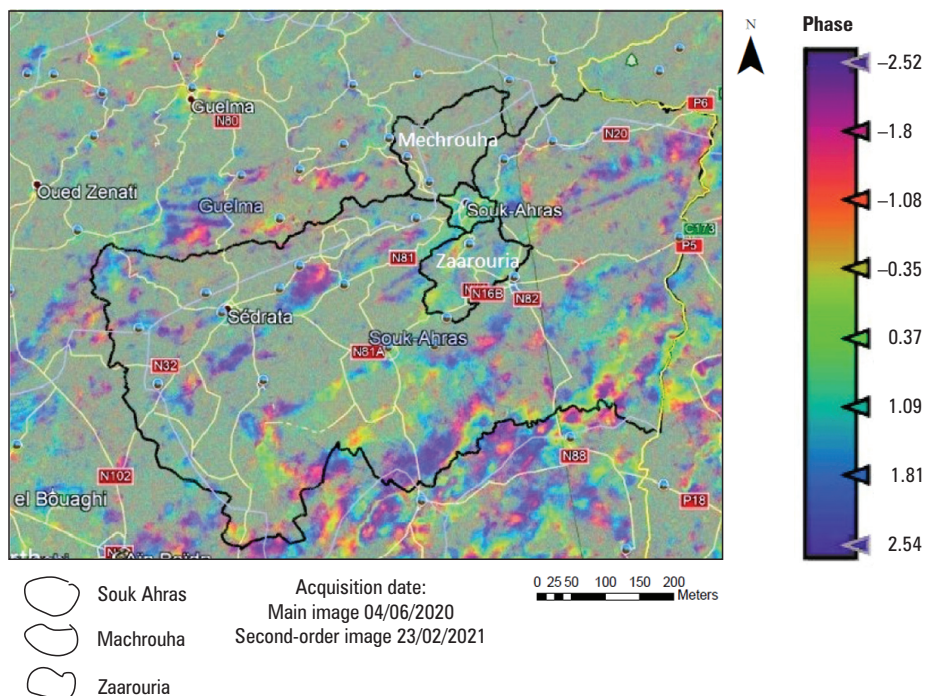


Source: Authors' own study

Fig. 11. The resulting product interferometry map

After the coregistration step, the interferogram was created. Pictures were adjusted and coordinated with a course taken by the DEM-assisted fine coregistration of sub-pixel

precision. The determined unique interferogram was utilized to run the topographic stage with the computerized rise show (DEM) that was naturally procured by the SNAP computer program in arrange to deliver a differential interferogram. The Goldstein stage channel was additionally overconnected to improve the created interferogram and make the interferometry borders outwardly clearer. After bringing in the comes about back in SNAP, the stage values were changed over to relocation values. In arrange to get exact results, geometric redress and coherence concealing were applied to lead to the ultimate yield, which was the uprooting outline. The result appeared in Figures 11–12.



Source: Authors' own study

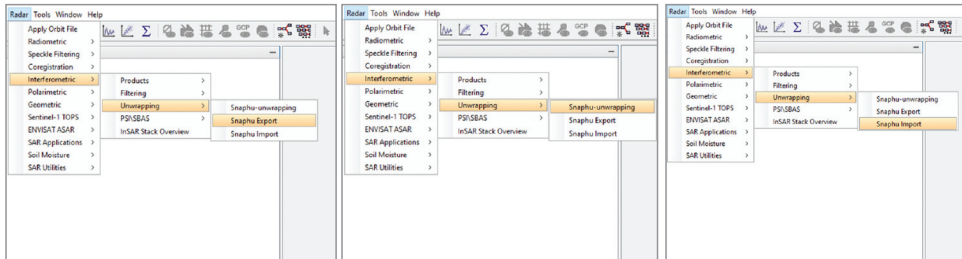
Fig. 12. The resulting product interferometry of Souk Ahras landslides

5.3.2. Phase unwrapping

The interferometry stage is equivocal and appears to be within the scale of 2π in the interferogram. It must first be unwrapped in order to connect it to the topographic stature. The elevation difference that results in a 2π change in interferometry stage after interferogram straightening is referred to as the height of uncertainty.

By coordinating the stage distinction between nearby pixels, stage unwrapping process recognizes this uncertainty. The stage difference between two focuses on the straightened interferogram gives an estimation of the real height variety in a similar manner after any number of heights of uncertainty have been removed (equivalent to

a number of 2 stage cycles), and unwrapped results should be translated as a relative height/displacement between pixels of two pictures (Fig. 13).



Source: Authors' own study

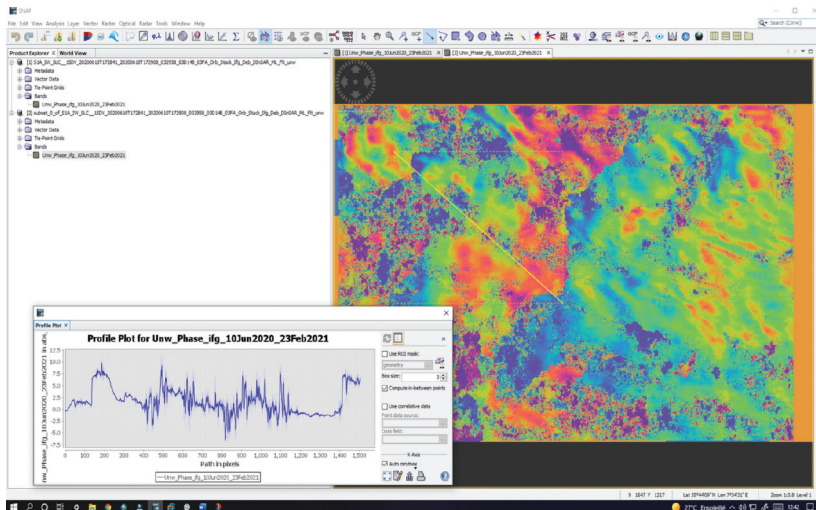
Fig. 13. Unwrapping steps

5.3.3. Unwrap the interferogram phase with snaphu

After the results are appropriately exported, SNAP's unpacking feature can be applied. In SNAP, there are three unique processes to unwrapping:

- 1) **snaphu export** of the wrapped phase (and definition of the parameters)
Radar \longrightarrow interferometric \longrightarrow unwrapping \longrightarrow snaphu export
- 2) **snaphu unwrapping** of the wrapped phase (performed outside SNAP by snaphu)
- 3) **snaphu import** of the unwrapped phase back into SNAP
Radar \longrightarrow interferometric \longrightarrow unwrapping \longrightarrow snaphu import

The result is shown in Figure 14.

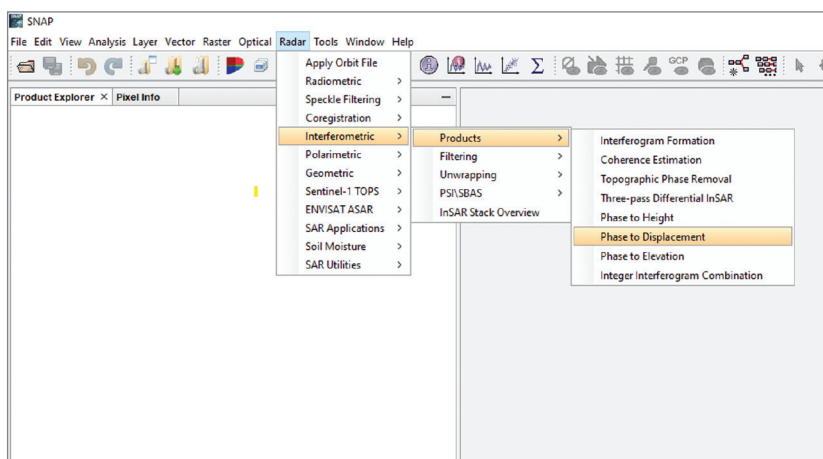


Source: Authors' own study

Fig. 14. Result of unwrapped phase

5.3.4. Steps to Create a Deformation Map

Although it is currently a continuous raster, the uprooting stage is not a metric degree yet. The Stage of Uprooting operator (under Radar > Interferometry > Items) (Fig. 15) is connected to convert radian units to ultimate relocations. It converts the stage into meters in terms of surface changes along the line of sight (LOS). The LOS is the measurement of the separation between a sensor and a pixel.



Source: Authors' own study

Fig. 15. Phase of displacement

Similar to how negative values sharply sink the surface, positive values sharply elevate (on the off chance that the ace picture has the prior procurement date).

The unwrapped stage that was imported in the last step is attached to the Phase to Displacement operator, which has no parameters. It generates a result that resembles the unwrapped stage (with a somewhat distinct predetermined color slope), but now each pixel has metrics showing its uprooting.

In this step, the unwrapped differential stage value (in radians) is converted to a relocation value (in meters) along the line of sight of the sensor location.

6. Results and discussion

6.1. Interferogram interpretation

The images were at first imported to the SNAP program. After checking that the combination of images was appropriate for the running assignment, the two images were coregistered within the SNAP environment. The interferometry stage carries a diversity of data including surface distortion (quality and course of movement), and the surface rupture area. The scene plot also mediates other earthquake-related parameters, such

as the vitality discharged during an event and the amount of shaking experienced in the affected area (Figs. 11 and 12). Interferograms appearing in concentrated stage weighted by the range of interferometry relationship have no relationship and critical stage discontinuities, which show 2π per colour cycle. (Figure 14) Interferograms appearing in concentrated interferometry stage (+: red, -: blue).

The determined interferogram, basically the contrast between the stages of two SAR images, is affected by the geology because it is strongly connected to the surface rise. In order to obtain a SAR interferogram without the surface rise impact, a DEM was applied to reenact the topographic borders (topographic stage), which were at that point evacuated from the delivered interferogram. Goldstein stage sifting was at that point carried out before the unwrapping as a preliminary step for expanding the signal-to-noise proportion. The differential interferogram created in past steps contains data concerning height relocation.

6.2. Image anomalies

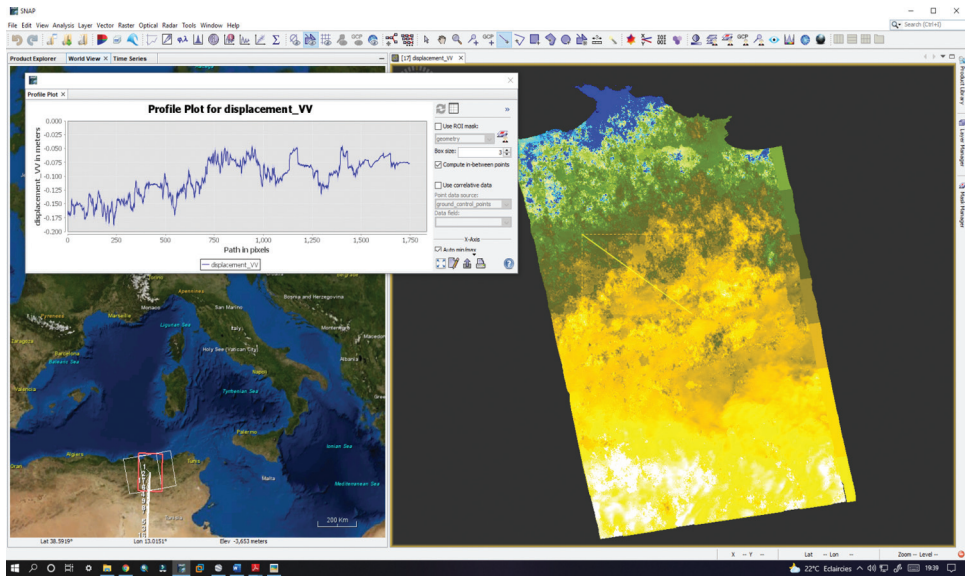
Some of the SAR images meet unavoidable radio recurrence obstructions from microwave sources on the ground transmitting within the same recurrence. This is often more common in sea settings, this phenomenon is also evident in the subsequent image in this SLC combine. Thus, this locale on the image will create wrong stage data. The coherence band will demonstrate this and give a strategy for concealing the inconsistency out of interferogram or afterward items utilizing band mathematics. On the other hand, selecting another SLC in an afterward point in time may diminish the coherence and quality of the complete interferogram.

6.3. Displacement interpretation

This investigation field estimation was able to identify ground surface distortion within the scope of the study area due to the deformation of the Earth's surface is in mm values extending from -0.108 and 0.012 , appear that negative surface distortion (subsidence) in shades of blue and shadow of green, watched in north-east and south-west parts of Souk Ahras range.

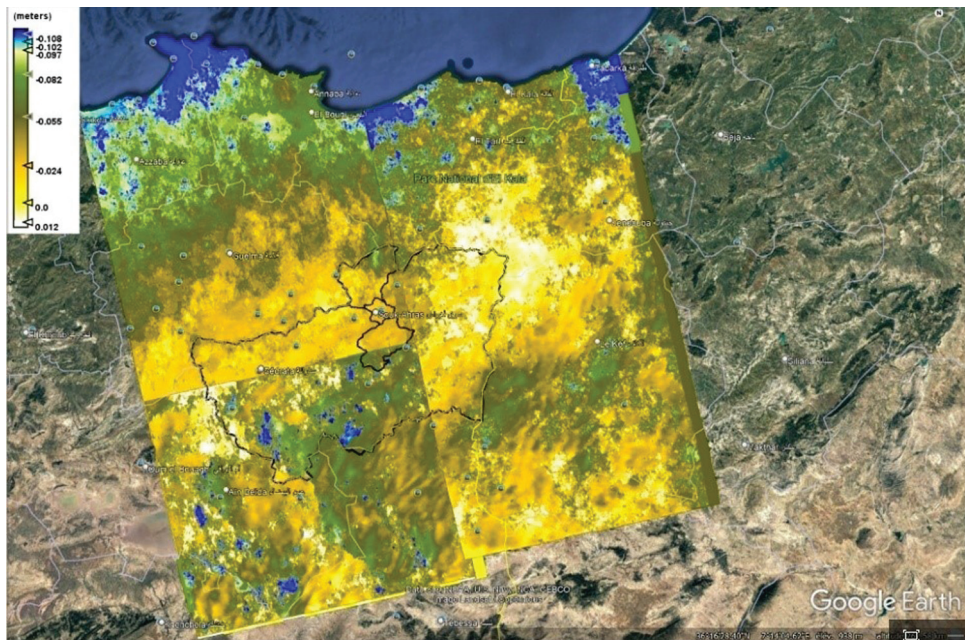
One can digitize a line to see single displacement patterns and their ranges using the Profile Plot tool (Fig. 16). This approach is beneficial for estimating the noise density in the lower coherence zones.

In this case the unwrapped phase, the subsidence is indicated up to -0.102 m. The shown orthorectified of the unwrapped stage interferogram and vertical uprooting layer were sent out to Google soil professional computer program, to create more clarity in the results. This allows us to come with a few insights to the geological area, which uncovered that significant surface distortion watched around Machrouha city (Fig. 17). Usually due likely, to the geographical nature of the soil (generally clayey soil), the topographic morphology is characterized by Triassic diapers and human causes.



Source: Authors' own study

Fig. 16. Profile plot for the displacement



Source: Authors' own study

Fig. 17. The resulting product displacement map. Result exported to Google Earth

7. Conclusion

These data within the frame of relocation maps can be utilized in the decision-making process of neighborhood partners and specialists, and it can be used for the real-time disaster/emergency administration for the safety of the environment and citizens. Such a kind of arrangement will allow the decision-makers to observe and prevent dangers of landslides in the shortest time possible. This data combined with risk maps showing the condition of the social legacy landmarks of intrigued can give specialists a necessary tool for taking specialized preventing measures for the particular landmarks based on their characteristics and dwelling dangers in each particular location.

In the future, interferometric stacking procedures, such as the examination of tireless scatterers, will be tested for distinct combinations of SAR image sets, like bottom-up or top-down image sets, for the global verification of ground deformations in the region of social heritage destinations. The application of interferometry stacking strategies will offer assistance to ponder the powerlessness of uncovered and/or buried social legacy landmarks to the residing site-specific dangers, and it'll help within the advancement of suitable helplessness maps that will help neighborhood specialists in embracing defensive measures to preserve the social and archaeological heritage.

References

- Akbarimehr M., Motagh M., Haghshenas M.** 2013. Slope Stability Assessment of the Sarcheshmeh Landslide, Northeast Iran, Investigated Using InSAR and GPS Observations. *Remote Sens.*, 5, 3681–3700.
- Bovenga F., Wasowski J., Nitti D.O., Nutricato R., Chiaradia M.T.** 2012. Using COSMO/SkyMed X-band and ENVISAT C-band SAR interferometry for landslides analysis. *Remote Sens. Environ.*, 119, 272–285.
- Cigna F., Bianchini S., Casagli N.** 2013. How to assess landslide activity and intensity with Persistent Scatterer Interferometry (PSI): The PSI-based matrix approach. *Landslides*, 10, 267–283.
- Chouabi A.** 1987. Etude géologique de la région de Hammam N'Bails SE de Guelma, Algérie. PhD thesis, Paul Sabatier, Toulouse University, France.
- Cruden D.M., Varnes D.J.** 1996. Landslides: Investigation and Mitigation. Chapter 3. Landslide Types and Processes. **Transportation Research Board Special Report. The National Academies of Sciences, Engineering, and Medicine.** Washington, DC, USA, 247.
- Frangioni S., Bianchini S., Moretti S.** 2014. Geomatics, Natural Hazards and Risk. Landslide inventory updating by means of Persistent Scatterer Interferometry (PSI): The Setta basin (Italy) case study. *Geomat. Nat. Hazards Risk*.
- Guzzetti F., Cardinali M., Reichenbach P., Carrara A.** 2000. Comparing Landslide Maps: A Case Study in the Upper Tiber River Basin, Central Italy. *Environ. Manag.*, 25, 247–263.
- Haghshenas Haghighi M., Motagh M.** 2016. Assessment of ground surface displacement in Taihape landslide, New Zealand, with C- and X-band SAR interferometry. *New Zeal. J. Geol. Geophys.*, 59, 136–146.
- Hanssen R.F.** 2001. Radar Interferometry – Data Interpretation and Error Analysis. *Journal of Physics A: Mathematical and Theoretical*.

- Kabouya M.** 1990. Modélisation pluie-débit aux pas de temps mensuel et annuel en Algérie septentrionale. PhD thesis. Paris Sud Orsay University.
- Masrouhi A., Ghanmi M., Ben Slama M.M., Ben Youssef M., Vila J.M., Zargouni F.** 2008. New tectono-sedimentary evidence constraining the timing of the positive tectonic inversion and the Eocene Atlasic phase in northern Tunisia: Implication for the North African paleo-margin evolution. *C.R. Geosci.*, 340, 771–778.
- Mebarki A.** 2003. Cartographie automatique des précipitations: application à l'Est algérien. *Sci. Technol. B*, 20, 100–107.
- Mebarki A.** 2005. Hydrologie des bassins de l'est algérien: ressources en eau, aménagement et environnement. PhD thesis. Mentouri University, Constantine, Algeria.
- Raucoules D., de Michele M., Aunay B.** 2020. Landslide displacement mapping based on ALOS-2/PALSAR-2 data using image correlation techniques and SAR interferometry: Application to the Hell-Bourg landslide (Salazie circle, La Réunion Island). *Geocarto Int.*, 35, 113–127.
- Riheb H., Khaled R., Larbi G., Abdelmadjid Ch., Younes H.** 2017. Slope Failure Characteristics and Slope Movement Susceptibility Assessment Using GIS in a Medium Scale: A Case Study from Ouled Driss and Machroha Municipalities, Northeast Algeria. *Arabian Journal for Science and Engineering*, 42 (1) 281.
- Rosenbaum G., Lister G.S., Duboz C.** 2002. Reconstruction of the tectonic evolution of the western Mediterranean since the Oligocene. *J. Virtual Explor.*, 8, 107–130.
- Sentinel Data Access Overview. Sentinel Online. <https://sentinel.esa.int/web/sentinel/sentinel-data-access> [accessed: 26 June 2019].
- SNAP. <https://step.esa.int/main/toolboxes/snap/> [accessed: 17 July 2019].
- VanWesten C.J., Van Asch T.W., Soeters R.** 2006. Landslide hazard and risk zonation. Why is it still so difficult? *Bull. Eng. Geol. Environ.*, 65, 167–184.
- Vila JM.** 1980. La chaîne alpine d'Algérie nord-oriental et des confins algéro-tunisiens. PhD thesis, P. et M. Curie, Pris VI University.
- Wasowski J., Bovenga F.** 2014. Investigating landslides and unstable slopes with satellite Multi Temporal Interferometry: Current issues and future perspectives. *Eng. Geol.*

PhD Nour El Houda Gueraidia
Department of Earth Sciences,
Tebessa University, Algeria
e-mail: nour.gueraidia@univ-tebessa.dz
ORCID: 0000-0003-4119-828X

PhD Saida Gueraidia
Department of Earth Sciences,
Tebessa University, Algeria
e-mail: saida.gueraidia@univ-tebessa.dz
ORCID: 0000-0001-6041-7201
Prof. Chemseddine Fehdi
Department of Earth Sciences,
Tebessa University, Algeria
e-mail: fehdi.chemseddine@univ-tebessa.dz